

# Extended X-Ray Absorption Fine Structure Study of Arsenic in HgCdTe

S. PLISSARD,<sup>1</sup> G. GIUSTI,<sup>1</sup> B. POLGE,<sup>1</sup> P. BALLET,<sup>1,3</sup> A. MILLION,<sup>1</sup>  
X. BIQUARD,<sup>2</sup> E. MOLVA,<sup>2</sup> JP. BARNES,<sup>1</sup> and P. HOLLIGER<sup>1</sup>

1.—CEA-LETI, MINATEC, 17 rue des Martyrs, 38054 Grenoble Cedex 9, France. 2.—DRFMC-CEA-Grenoble, 17 rue des Martyrs, 38054 Grenoble Cedex 9, France. 3.—e-mail: philippe.ballet@cea.fr

Extended x-ray absorption fine structure (EXAFS) experiments using the As *K*-edge have been carried out at the European Synchrotron Radiation Facility on two molecular beam epitaxy (MBE) grown arsenic-doped HgCdTe samples. Arsenic (As) is provided by a radio-frequency plasma cell and was incorporated to a level of a few  $10^{18}$  at·cm<sup>-3</sup>. Both samples were analyzed as grown and after a high-temperature anneal (410°C/1 h) under saturated mercury pressure. The EXAFS signature of as-grown and annealed samples are strikingly different, indicating a drastic change in the environment of the As atom. In any case, the EXAFS signal originates from at least two different contributions and is found to be dominated by As clusters. The other contribution for as-grown samples comes from tellurium neighbors indicating that As incorporates partially in the (Cd,Hg) site.

**Key words:** Extended x-ray absorption fine structure (EXAFS), HgCdTe

## INTRODUCTION

Mercury cadmium telluride is the material of choice for developing high-performance infrared photo-detectors. The increasing demand in detector flexibility and performance has considerably broadened the field of application covered by these detectors but also increased the complexity of detector structures.<sup>1-5</sup> Today, the realization of such detectors involves the complete control of alloy composition and doping. Whereas *n*-type doping using indium is well matured, the extrinsic *p*-type doping is still under development and usually requires thermal activation of column V elements.<sup>6,7</sup> Arsenic (As) is often chosen as the best candidate for both postgrowth ion implantation doping and *in-situ* incorporation.<sup>8-10</sup> This is for several reasons such as the low diffusion coefficient and the availability of mature molecular beam epitaxy (MBE) technology developed for the III-V industry.<sup>11</sup>

The goal of this paper is to investigate the chemical environment of As when incorporated into an HgCdTe zinc-blende crystal. Extended x-ray absorption fine structure (EXAFS) is therefore used to probe the distances and chemical nature of As neighbors in the lattice. This powerful technique is used to study As incorporated by MBE using a nonconventional plasma cell. The effect of high-temperature thermal annealing on the EXAFS signature is also considered. Thermal annealing is believed to enhance the fraction of Te-substitutional As by thermally activating a change of crystal site, although the exact mechanism is a matter of debate.<sup>6,7,12,13</sup>

The paper is organized as follows. In the first section, we present the preparation and characterization of the samples used for the EXAFS runs. The second section is dedicated to the EXAFS experiment itself, presenting the basic setup and the main experimental results. In the third section, we will discuss the EXAFS results in light of first-principle calculations, and we will compare the results with some current theories for As incorporation and thermal activation.

## SAMPLE PREPARATION AND CHARACTERIZATION

### MBE-Grown Samples

Arsenic-doped HgCdTe layers were grown in a Riber 32P chamber using conventional effusion cells for Hg, Cd, and Te elements and a radio-frequency (RF) plasma cavity for As. In such a configuration, As molecules are expected to be cracked down to atomic As. The HgCdTe growth is initiated at 180°C on a CdZnTe (211)B surface. The layers are typically 6- $\mu\text{m}$  thick, doped with As and terminated by an undoped cadmium-rich thin cap layer. The cadmium composition of the doped layer is 0.3. High-resolution x-ray diffraction has been systematically used to check on the crystal quality of both substrates and HgCdTe layers. Full-width at half-maximum of the HgCdTe layer diffraction peak is in the 40–70 arcsec range depending on the CdZnTe substrate. These values are similar to what is commonly measured on undoped As layers, indicating no degradation of the crystalline quality due to the presence of As. This result is further confirmed by chemical revelation of emerging dislocations both on the cap-layer surface and on the doped HgCdTe layer after removal of the cap layer using bromine etch. The etch pit density is in the very low  $10^5 \text{ cm}^{-3}$  and is found to be systematically larger when measured on the cap-layer due to lattice mismatch induced by the increase in cadmium composition. For EXAFS measurements, two samples have been considered, namely, samples A and B. The main material characteristics are listed in Table I. Samples A and B are equivalent except for the differences in the As reservoir temperature.

### Annealing Process

All samples have been cleaved into two with one of the two pieces dedicated to the study of the thermal annealing process. The anneal has been shown to be very effective in electrically activating As as an acceptor impurity.<sup>6,7</sup> Anneals at a dwell temperature of 410°C have been performed for 1 h under saturated mercury pressure conditions. This high-temperature anneal is followed by a low-temperature anneal (200°C) for drastic reduction of the density of mercury vacancies generated during the high-temperature anneal.

### Diffusion Induced by High-Temperature Annealing

High-temperature annealing, in addition to enhancing the activation of As, may change the composition profile of heterostructures due to the diffusion of the main constituents such as Cd, Hg, and Zn and, of course, As. Even though the structures studied here are rather simple, it is still of interest to investigate what happens at the substrate/layer and layer/cap-layer interfaces. Infrared transmission provides direct evidence that the composition profile is changed by high-temperature annealing. Figure 1 shows three different infrared transmission spectra for sample B, obtained right after growth, after a low-temperature anneal (200°C) and a high-temperature anneal. All of these spectra have been obtained on the same sample. As expected, a low-temperature anneal does not modify the structure, whereas a high-temperature anneal strongly affects the shape of the spectrum. The changes in the FTIR spectrum are (1) a significant blue shift of the cut-off wavelength, indicating an increase in the overall cadmium composition; (2) a smoother absorption front typical of a graded composition profile; and (3) a significant decrease in the amplitude of the interference oscillations in the

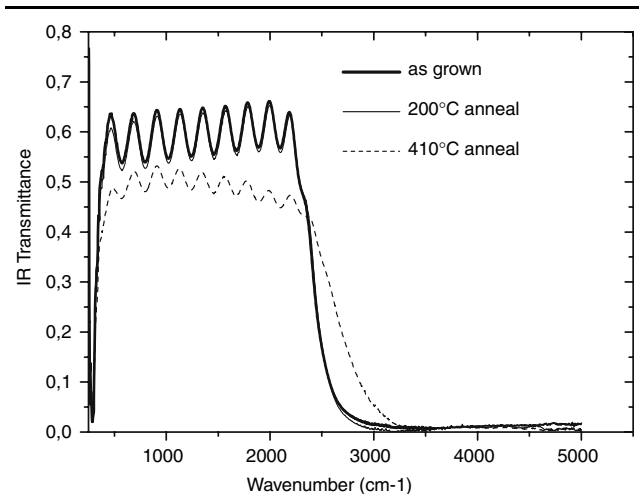


Fig. 1. Room-temperature FTIR spectra for sample B. FTIR spectrum obtained right after growth is plotted in the bold line. The spectra for low-temperature (200°C) and high-temperature (410°C) annealed samples are plotted with the thin solid line and dashed line, respectively.

Table I. Main Specifications of the Samples Used for EXAFS Investigation

Sample	As Reservoir Temperature (°C)	RF Cavity Power (W)	Thickness of the As-Doped Layer ( $\mu\text{m}$ )	Cadmium Fraction
A	320	500	6.0	0.30
B	340	500	6.0	0.30

transparent region, witnessing an alteration of the substrate-layer interface.

Secondary ion mass spectroscopy (SIMS) gives additional information as to how the high-temperature anneal affects the Cd, Hg, Zn, and As depth profiles. The SIMS depth profiles were obtained using a CAMECA 5F magnetic sector SIMS with a 2 keV Cs beam incident at 50° to the sample normal. Positive secondary ions were measured in the form  $MCs^+$ , where M is the element of interest combined with Cs from the analysis beam to form a positive molecular ion. Figure 2 shows the SIMS spectra for sample B, either (a) as grown or (b) after the 410°C anneal. The SIMS signals from surface to substrate have been normalized to the tellurium

signal and corrected for matrix effects (HgCdTe and CdZnTe). The As incorporation is found to be rather inhomogeneous in depth with a significant increase of the As density close to the layer/substrate interface. This effect originates from a burst effect in the plasma cell. The peak level for As is  $7 \cdot 10^{19} \text{ cm}^{-3}$ . After the burst, the As signal stabilizes at a value of about  $1 \cdot 10^{18} \text{ cm}^{-3}$ . Of course, for EXAFS investigation, the material affected by the burst of As will have a prominent response, because there are no other contributions to the EXAFS signal, at the As edge, except from As atoms.

The zinc signal is normalized assuming a zinc content of 4% in the substrate. From the two sets of profiles, it is evident that the annealing process deeply modifies Cd, Hg, and Zn fractions throughout the entire structure. Cadmium strongly diffuses from the substrate and the cap layer toward the HgCdTe layer, resulting in a strongly graded structure. Zinc also diffuses from the substrate and penetrates the HgCdTe layer to a thickness of about 2  $\mu\text{m}$ . Finally, As does not seem to diffuse much, which is consistent with its very low diffusion coefficient.<sup>11</sup> All of these observations are consistent with the FTIR data presented earlier and point out the importance of thermal diffusion in HgCdTe heterostructures. Further study of the diffusion of Cd and Zn shows that decreasing the annealing temperature to 320°C or reducing the annealing time to 10 min almost totally suppresses the diffusion process.

Table II summarizes the SIMS data for As concentrations in as-grown and 410°C annealed samples. The FTIR derived cut-off wavelength at 300 K is also listed for as-grown and annealed samples as a measure of the absorption front shift induced by cadmium and zinc diffusion.

Despite the significance of diffusion caused by the thermal annealing process and the impact on the optical data, we expect these compositional modifications to have very little impact on the EXAFS signature. This is because the matrix is still HgCdTe with a slightly different cadmium composition. No As diffusion inside the substrate or the cap layer, where the cadmium and mercury fraction are really different, has been observed. There is only a weak As diffusion from the burst peak to the plateau region. This can be seen from the data in Table II; the peak level decreases for annealed samples, while the plateau level slightly increases.

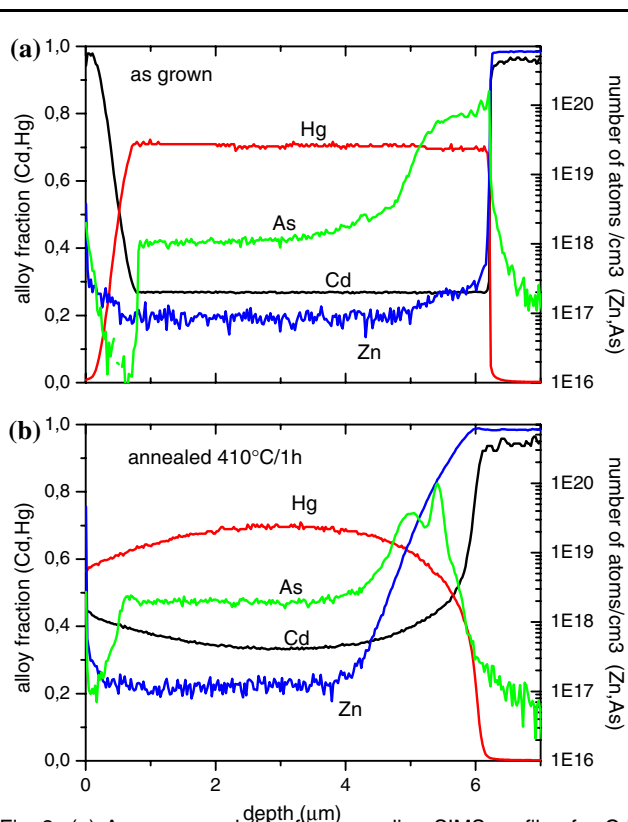


Fig. 2. (a) As grown and (b) after annealing SIMS profiles for Cd, Hg, As, and Zn. The substrate is on the right-hand side of the figure, while the sample surface is on the left. Cadmium and mercury signals are plotted in the alloy fraction (left scale), and As and zinc signals are in atoms per cubic centimeter (right scale).

**Table II. SIMS Data for All Samples Investigated (Annealed and As-Grown)**

Sample	As Level at Peak ( $\text{at}/\text{cm}^3$ )	As Level at Plateau ( $\text{at}/\text{cm}^3$ )	Cut-Off Wavelength 300 K ( $\mu\text{m}$ )
A as-grown	$8.0\text{E} + 19$	$1.8\text{E} + 17$	4.10
A annealed	$5.0\text{E} + 19$	$3.0\text{E} + 17$	3.60
B as-grown	$7.5\text{E} + 19$	$1.1\text{E} + 18$	4.16
B annealed	$3.5\text{E} + 19$	$1.9\text{E} + 18$	3.86

## EXAFS EXPERIMENTS

X-ray absorption spectroscopy (XAS) experiments were performed at the FAME beamline (BM30B) at the European Synchrotron Radiation Facility in Grenoble. The XAS spectra were recorded at the As *K*-edge (11866.7 eV) in fluorescence mode with a 30-element energy-resolved detector. Experiments were conducted at room temperature, and the  $200 \times 300 \mu\text{m}^2$  x-ray spot was kept centered on the As:HgCdTe sample (size  $> 10 \times 10 \text{mm}^2$ ) during energy scans by dynamically adjusting the curvature of the second crystal of the Si(220) monochromator and tracking the beam height. Good harmonic rejection and maximal resolution is achieved thanks to two Rh-coated mirrors of adjustable tilt and curvature located on both sides of the monochromator. The incidence angle of the x-ray beam on the sample surface was kept constant at around  $45^\circ$ . Energy calibration was made using the  $\text{As}_2\text{O}_3$  powder edge (11,869 eV). Base line extraction of XAS spectra was done using the ATHENA program,<sup>14</sup> and EXAFS analysis was conducted using the FEFF and FEFFIT package programs.<sup>15</sup>

The EXAFS is a very local probe because its range of investigation is basically limited to a distance of 6–8 Å from the probed As atom. Therefore, EXAFS is only sensitive to the first neighbors surrounding As. In principle, the chemical nature of these neighbors as well as their distance to the As atom can be extracted from EXAFS spectra through mathematical treatment and comparison with first-principles calculations. Practically, the detection limit for reasonable photon counting time and signal-to-noise ratio has been found to be for an As density near  $5 \cdot 10^{17} \text{cm}^{-3}$  because of the intrinsic sensitivity to As but also because of the presence of the mercury absorption edge.

## EXAFS RESULTS AND DISCUSSION

A typical absorption spectrum is displayed in Fig. 3. After the As absorption edge, the EXAFS oscillations are clearly visible and expand up to the onset of the mercury edge (12,240 eV). As the Hg edge onset limits the EXAFS range due to the prominence of the mercury atoms in the investigated structures, a 3- $\mu$  thick Ge foil (*Z*-1 of As) was placed in front of the fluorescence detector to send the Hg edge onset as far as possible. Studied samples A and B show a constant absorption edge energy position equal to  $11,866.5 \pm 0.25 \text{eV}$ , thus indicating that As is essentially neutral.<sup>16</sup>

The EXAFS oscillation  $\chi(k)$  results from the removal of the baseline underlying the absorption spectrum, as illustrated in Fig. 4. Once amplified for easier treatment, Fourier transformation leads to the pseudo-distance of neighbors around As atom  $|\chi(R)|$ . Because of the presence of the mercury

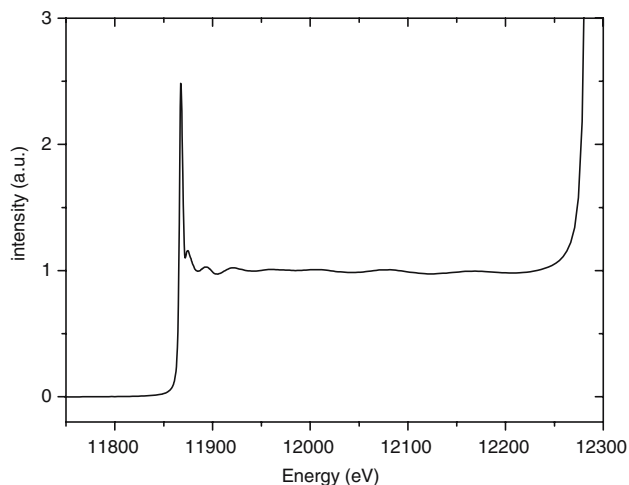


Fig. 3. EXAFS spectrum for sample B (as-grown) as a function of incident photon energy.

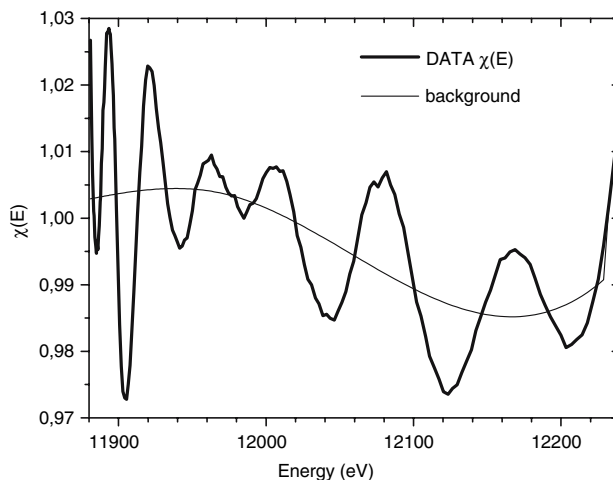


Fig. 4. EXAFS oscillation extraction using Athena. A background  $R$  of 1.2 Å has been used.

absorption edge, *k*-space analysis is limited in our case to  $10 \text{Å}^{-1}$ .

Figure 5 compares, for samples A and B *k*, the  $\chi(k)$  EXAFS oscillations, while Fig. 6 compares  $|\chi(R)|$ . As can be seen in Figs. 5 and 6, there is a major effect of thermal annealing on EXAFS oscillations. The EXAFS oscillations of annealed samples are completely different from those of as-grown samples: annealing has completely changed the local environment of As.

Figure 6 shows that this is associated with the dominant contribution (first double peak for  $RE[1.4\text{--}2.8 \text{Å}]$ ) becoming a single peak and a second peak around  $R = 3.4 \text{Å}$  appearing: associated high-frequency oscillations are clearly visible on annealed spectra and indicate that annealing leads to a better ordering around As. As the first peak between  $RE[1.4\text{--}2.8 \text{Å}]$  is double, As in not-annealed samples has two different chemical environments. Figure 5

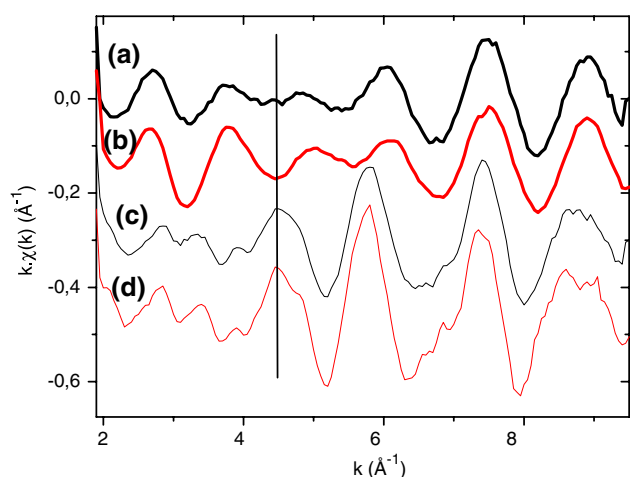


Fig. 5. Comparison between EXAFS oscillations  $k\chi(k)$ : (a) and (b) samples A and B before annealing, respectively; and (c) and (d) samples A and B after 410°C annealing, respectively. Spectra have been shifted down for clarity. The vertical bar at  $k = 4.5 \text{ \AA}^{-1}$  marks the boundary between low- $k$  and high- $k$  contributions.

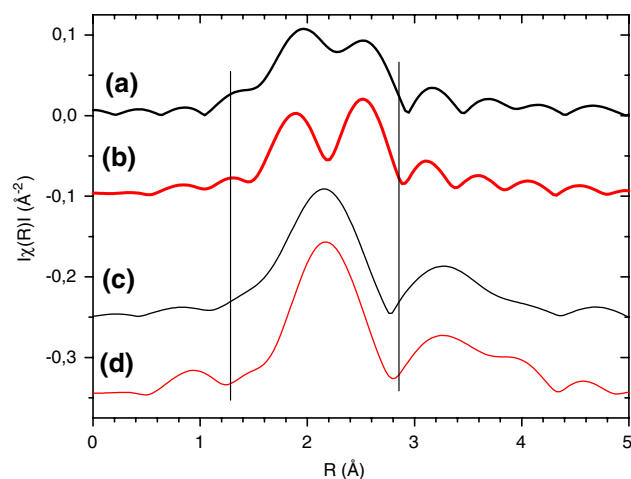


Fig. 6. Comparison between EXAFS oscillations  $I\chi(R)$ : (a) and (b) samples A and B before annealing, respectively; and (c) and (d) samples A and B after 410°C annealing, respectively. Spectra have been shifted down for clarity. The vertical bars show the  $R$  range selected for Fourier back-transform data fitting.

shows that EXAFS oscillations of samples A and B before annealing are made, in fact, of the two same contributions but with different relative intensity: the low- $k$  contribution ( $k$  value below vertical bar) is more intense for sample B compared to sample A and vice-versa for the high- $k$  contribution.

The EXAFS analysis was conducted on the Fourier back-transformed oscillations  $\text{Re}[\chi(q)]$  and was able to identify the two different chemical environments of the not-annealed As sample. Fit adjustment values are given in Table III. As a consequence of the reduced available  $k$ -range, we had to limit the number of adjustment parameters for

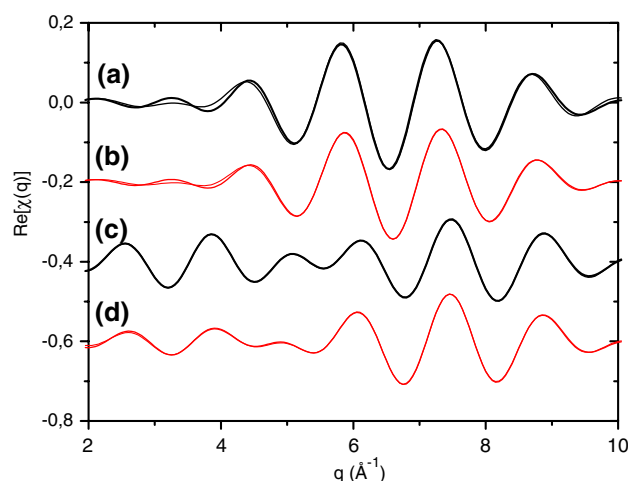


Fig. 7. Comparison between EXAFS oscillations  $\text{Re}[\chi(q)]$  and associated fits. Data curves are in bold solid lines, while fitting curves are in thin solid lines. Most of the fits are indistinguishable from the data. Curves (data and fit): (a) and (b) samples A and B before annealing, respectively; and (c) and (d) samples A and B after 410°C annealing, respectively. Spectra have been shifted down for clarity.

the two contributions of not-annealed sample. We chose to have a single energy offset  $\Delta E$  and a single Debye–Waller  $\sigma^2$  parameter for both contributions. Also, it was not possible to have a sufficiently correct fit for the peak at  $R = 3.4 \text{ \AA}$  for annealed A and B samples. Figure 7 shows a comparison between experiment and fit, the agreement between experiment and fit being excellent.

For each adjustment, a small and rather constant energy shift  $\Delta E$  (eV) #4 eV was found, consistent with neutral As. The EXAFS analysis clearly identifies the two contributions: the first one comes from Te being at 2.65 Å and the second one from As being at 2.46 Å. Moreover, the amplitude of the Te contribution is larger for sample B than for sample A.

The first contribution probably indicates that As has incorporated inside HgCdTe by substituting in the (Hg,Cd) site. This result was expected because MBE growth occurs under tellurium-rich conditions, thus favoring cadmium or mercury vacancies. This also confirms that, immediately after growth, As acts as a donor rather than an acceptor. In the case of a single contribution, As should have 4 Te as first neighbors. Therefore, (Hg,Cd) substitution only concerns one-fifth of As in sample A and one-third in sample B. As (Hg,Cd)-Te distance in HgCdTe is 2.78 Å; this substitution of (Hg,Cd) takes place with a 1% contraction of bond length. To demonstrate more clearly the substitutional nature of As on the (Hg,Cd) site, we have tried to find a second shell surrounding the As made up only of (Hg<sub>0.7</sub>,Cd<sub>0.3</sub>) neighbors, but the much more intense second contribution prevented us from succeeding.

This second contribution is made of As-As first neighbors, indicating that most incorporated As are linked to another As. This is not surprising considering

Table III. Adjustment Values for Data Fit of As:HgCdTe Samples A and B\*

R Range of Back-Transform	Nature	Number	Distance (Å)	$\sigma^2$ ( $10^{-3}\text{Å}^2$ )	$\Delta E$ (eV)
<b>Before Annealing</b>					
[1.5:3.0 Å] Sample A					
First contribution	Tellurium	$0.85 \pm 0.2$	$2.65 \pm 0.05$	$3.0 \pm 2$	$4.7 \pm 1.3$
Second contribution	As	$2.0 \pm 0.5$	$2.46 \pm 0.02$	Same	Same
Sample B					
First contribution	Tellurium	$1.3 \pm 0.1$	$2.63 \pm 0.01$	$3.2 \pm 0.5$	$3.2 \pm 0.3$
Second contribution	As	$1.6 \pm 0.1$	$2.46 \pm 0.01$	Same	Same
<b>After annealing, k &gt; 4.4</b>					
[1.4:2.8 Å] Sample A	As	$4.6 \pm 1.5$	$2.49 \pm 0.06$	$7.4 \pm 3.4$	$4.9 \pm 3.8$
Sample B	As	$7.2 \pm 2.6$	$2.52 \pm 0.07$	$10.3 \pm 3.9$	$5.7 \pm 4.2$

\*The reduction factor  $S_0^2$  was fixed to 0.8;  $\sigma^2$  is the Debye–Waller factor, which measures the damping of EXAFS oscillations coming from either thermal agitation or crystal disorder; and  $\Delta E$  is the energy offset between experimental and first-principles calculated Fermi levels.

the fact that As in the plasma cell burst may well recombine with other As atoms at the growing surface because of the very large As flux during this transitory phenomenon. Once annealed, only As neighbors are visible, in large number with an average distance of 2.5 Å, indicating the formation of subclusters of As inside HgCdTe. Also, the Debye–Waller  $\sigma^2$  parameter increases from  $3 \cdot 10^{-3} \text{Å}^2$  to more than  $7 \cdot 10^{-3} \text{Å}^2$ , indicating the formation of an amorphous As subcluster, thus allowing for more than 3 As as first neighbors as in the crystal.

### CONCLUSIONS

In summary, this EXAFS investigation of As-doped MBE samples shows that As incorporates both substitutionally in the place of a cadmium or a mercury atom and in the form of As clusters. High-temperature (above 400°C), mercury-saturated thermal annealing deeply changes the EXAFS signature, which becomes clearly dominated by the cluster contribution. At this point, it is not clear whether this cluster contribution originates from the burst region where the As concentration exceeds  $10^{19} \text{at}\cdot\text{cm}^{-3}$ ; further experiments, with homogeneously doped samples, are definitely needed to clarify this fundamental point.

### ACKNOWLEDGEMENTS

This work has been supported by the French Ministry of Defense (DGA). One of the authors (XB)

thanks O. Proux for the efficient help in solving EXAFS analysis.

### REFERENCES

1. P. Tribolet, J.P. Chatard, P. Costa, and S. Paltrier, *J. Electron. Mater.* 30, 574 (2001).
2. S. Velicu, G. Badano, Y. Selamet, C.H. Grein, J.P. Faurie, S. Sivananthan, P. Boieriu, D. Rafol, and R. Ashokan, *J. Electron. Mater.* 30, 711 (2001).
3. G. Destefanis, et al., *J. Electron. Mater.* 32, 592 (2003).
4. L.A. Almeida, M. Thomas, W. Larsen, K. Spariosu, D.D. Edwall, J.D. Benson, W. Mason, A.J. Stoltz, and J.H. Dinan, *J. Electron. Mater.* 31, 669 (2002).
5. J. Beck, C. Wan, M. Kinch, J. Robinson, P. Mitra, R. Scritchfield, F. Ma, and J. Campbell, *J. Electron. Mater.* 35, 1166 (2006).
6. M. Zandian, A.C. Chen, D.D. Edwall, J.G. Pasko, and J.M. Arias, *Appl. Phys. Lett.* 71, 2815 (1997).
7. P. Boieriu, C.H. Grein, H.S. Jung, J. Garland, and V. Nathan, *Appl. Phys. Lett.* 86, 212106 (2005).
8. L.A. Almeida, *J. Electron. Mater.* 31, 660 (2002).
9. P.S. Wijewarnasuriya and S. Sivananthan, *Appl. Phys. Lett.* 72, 1694 (1998).
10. E.C. Piquette, D.D. Edwall, D.L. Lee, and J.M. Arias, *J. Electron. Mater.* 35, 1346 (2006).
11. P. Capper, in *Properties of Narrow Gap Cadmium Based Compounds*, EMIS Datareviews (United Kingdom: INSPEC, 1994).
12. H.R. Vidyath, *Semicond. Sci. Technol.* 5, S213 (1990).
13. M.A. Berding and A. Sher, *Appl. Phys. Lett.* 74, 685 (1999).
14. B. Ravel and M. Newville, *J. Synchrotron. Rad.* 12, 537 (2005).
15. J.J. Rehr and R.C. Albers, *Rev. Mod. Phys.* 72, 621 (2000).
16. A. Foster, G. Brown, Jr., T. Tingle, and G. Parks, *Am. Mineral.* 553 (1998).